Evidence of magnetic field switch-off in PIC simulations of collisionless magnetic reconnection with guide field

M. E. Innocenti

Center for mathematical Plasma Astrophysics, Department of Mathematics, K.U. Leuven (University of Leuven), Celestijnenlaan 200B, B-3001 Leuven, Belgium

mariaelena.innocenti@wis.leuven.be

M. Goldman

Center for Integrated Plasma Studies, University of Colorado Boulder, Gamow Tower, Boulder, 80309-0390 Colorado, USA

martin.goldman@Colorado.edu

D. Newman

Center for Integrated Plasma Studies, University of Colorado Boulder, Gamow Tower, Boulder, 80309-0390 Colorado, USA

david.newman@colorado.edu

S. Markidis

PDC Center for high Performance Computing, KTH Royal Institute of Technology, Teknikringen 14, 10044 Stockholm, Sweden

markidis@kth.se

G. Lapenta

Center for mathematical Plasma Astrophysics, Department of Mathematics, K.U. Leuven (University of Leuven), Celestijnenlaan 200B, B-3001 Leuven, Belgium

giovanni.lapenta@wis.kuleuven.be

September 28, 2016

Received _____; accepted _____

ABSTRACT

The long term evolution of large domain Particle In Cell simulations of collisionless magnetic reconnection is investigated following observations that show two possible outcomes for collisionless reconnection: towards a Petschek-like configuration (Gosling 2007) or towards multiple X points (Eriksson et al. 2014). In the present simulation, a mixed scenario develops. At earlier time, plasmoids are emitted, disrupting the formation of Petschek-like structures. Later, an almost stationary monster plasmoid forms, preventing the emission of other plasmoids. A situation reminding of Petschek's switch-off then ensues. Switch-off is obtained through a slow shock / rotational discontinuity compound structure. Two external slow shocks located in correspondence of the separatrices reduce the in plane tangential component of the magnetic field, but not to zero. Two transitions reminding of rotational discontinuities in the internal part of the exhausts then perform the final switch-off. Both the slow shocks and the rotational discontinuities are characterized as such through the analysis of their Rankine-Hugoniot jump conditions. A moderate guide field is used to suppress the development of the firehose instability in the exhaust.

1. Introduction

Magnetic reconnection converts stored magnetic energy into kinetic energy and heat in a variety of heliospheric and astrophysical settings. The Sweet-Parker model predicts reconnection rates too slow to fit the observed values in solar flares and the solar corona (Priest & Forbes 2007). In Petschek's model for fast magnetic reconnection, two back-to-back slow shocks are the main sites of energy conversion. The size of the

diffusion region is reduced and fast reconnection is achieved (Vasyliunas 1975). Petschek's model for collisional plasmas is supported by MagnetoHydroDynamics simulations with non-homogeneous resistivity (Sato & Hayashi 1979). Another possibility for fast collisional magnetic reconnection is the plasmoid instability, triggered when an elongated Sweet-Parker layer becomes unstable to tearing-like modes (Loureiro et al. 2007; Lapenta 2008; Loureiro et al. 2012). It develops in simulations of collisionless plasmas also (Daughton et al. 2006; Drake et al. 2006a; Markidis et al. 2013). In collisionless plasmas, fast reconnection is achieved through the Hall effect (Birn et al. 2001). Effort has been put into understanding if collisionless reconnection can eventually reach a Petschek-like state, but results have been up to now inconclusive. Slow shocks develop in hybrid reconnection simulations (but Nakamura et al. (1998) disagrees). However, switch-off (i.e., the reduction to zero of the in plane tangential component of the magnetic field) is not observed (Krauss-Varban & Omidi 1995; Lin & Swift 1996a; Lottermoser et al. 1998; Arzner & Scholer 2001).

The hybrid community agrees that slow shocks develop at large distances (hundreds of ion skin depths, d_i) from the X point into the exhaust and at long simulated times (Higashimori & Hoshino 2012). For this reason, Particle In Cell (PIC) simulations, which are more computationally expensive than their hybrid counterparts, were long sidelined in the discussion. Recently, thanks also to new co-design (Lapenta et al. 2014 - accepted) and algorithmic (Innocenti et al. 2013; Beck et al. 2014; Innocenti et al. 2015) approaches, the scales covered by PIC simulations have started reaching the ones needed to observe the formation of shocks.

Contrasting observations of magnetic reconnection in collisionless environment exist. Gosling (2007) observes Petschek-like exhausts in the (collisionless) solar wind. Hones et al. (1984); Eriksson et al. (2014) instead describe multiple X points separated by plasmoids. It seems therefore that the single X point collisionless model may move either towards a single X point Petschek-like model or towards a multiple X point model (plasmoid formation) in the

phase diagram of Ji & Daughton (2011). The aim of the present paper is to contribute to clarifying the issue.

We build over the work of Liu et al. (2012) which shows that, in anti-parallel PIC reconnection, the exhaust boundary is made up of two slow shocks and a rotational wave. Switch-off is prevented by the development of the firehose instability, driven by the building up of ion parallel pressure. Karimabadi et al. (1999) and Le et al. (2013) show that a guide field (Kleva et al. 1995; Ricci et al. 2004) suppresses the firehose instability. Here, the simulation of Liu et al. (2012) is augmented by a moderate guide field with this purpose. Plasmoids are emitted during the early phase of the simulation. Plasmoid emission contrasts the formation of a Slow Shock/ Rotational Discontinuity (SS/RD) structure. The structure develops earlier in the rightwards exhaust which is not disrupted by the emission of medium-size plasmoids. It develops in the leftwards exhaust too when a big, almost stationary monster plasmoid (Uzdensky et al. 2010; Loureiro et al. 2012) forms at the initial X point and prevents the emission of the medium-size plasmoids previously emitted leftwards. Two slow shocks (SS) located at the upper and lower separatrices reduce the in plane tangential component of the magnetic field, but not to switch-off. The in plane tangential magnetic field is switched-off by transitions more internal to the exhaust and reminding of rotational discontinuities (RD). The formation of internal rotational discontinuities in PIC simulations with guide field has been hinted at (but not observed) in Liu et al. (2012). It has been observed by Lin & Swift (1996b) in 2D hybrid simulations of magnetic reconnection with guide field.

Compound SS/RD structures are observed in the solar wind, but there the RDs constitute the external transitions (Gosling et al. 2005).

2. Simulation setup

A 2D3V PIC simulation of collisionless magnetic reconnection is investigated. The domain is $L_x/d_i \times L_y/d_i = 819.2 \times 409.6$. 8192×4096 cells in the x (horizontal) and y (vertical) direction are used. A double Harris equilibrium (Harris 1962) is used as initial condition. One reconnection point is initialized, through a perturbation of the magnetic field with maximum value equal to $0.4B_0$ (B_0 is the peak field value in the x direction), at $(x'/d_i,\ y'/d_i) = (L_x/2,\ L_y/4)$. For convenience, the axes are translated to have it centered at $(x/d_i, y/d_i) = (0\ , 0)$ at initialization. The upper current sheet is left unperturbed. Boundary conditions are periodic for both fields and particles. Compatibly with Liu et al. (2012), the ion to electron mass ratio is $m_r = 25$, the half-width of the Harris sheet is $L_H/d_i = 2$, the ion (i) to electron (e) temperature ratio is $T_i/T_e = 1$ and the electron thermal velocity is $v_{th,e}/c = 0.16667$, where c is the speed of light. A background population of electrons and ions with density $\rho_{bg}/\rho_0 = 0.2$, where ρ_0 is the initial density for the streaming species, is also loaded. 108 particles per cell are used. The time step is $\Omega_{ci}\ dt = 0.01$, where Ω_{ci} is the ion cyclotron frequency. The code used is the semi-implicit code iPic3D (Markidis et al. 2010), routinely used for massive 3D simulations, e.g. Olshevsky et al. (2013).

3. Results

The large scale long term evolution of the simulation can be appreciated in the movie of the out of plane electron current provided as supplementary material. The unperturbed upper current layer evolves into a plasmoid chain at $\Omega_{ci}t > 190$. Plasmoid chains are observed in the terrestrial magnetotail and pause and in the solar corona (Lin et al. 2008). Reconnection in the lower current sheet is seeded by the perturbation and starts immediately

in a single X point configuration. The perturbation is used, as explained in Birn et al. (2001), to drive the lower current sheet into the non ideal regime of reconnection, skipping the plasmoid/ tearing phase observed in the unperturbed layer. Karimabadi et al. (2005) is referred for a study of the evolution of a multimode tearing unstable current layer into a single reconnection point.

When no guide field is used, the evolution of Liu et al. (2012) is recovered in the lower current sheet. With a guide field $B_g = 0.3B_0$, the firehose instability is suppressed. Plasmoids (Daughton et al. 2006; Drake et al. 2006b) are ejected asymmetrically into the leftwards (medium size plasmoids, with radius $r/d_i \sim 2$) and rightwards (smaller plasmoids, with radius $r/d_i \sim 0.5$) exhausts. The medium size plasmoids emitted leftwards disrupt the formation of the SS and RD structures in the leftwards exhaust. Similar breaks of the left-right symmetry are observed, for example, in Keppens et al. (2013) and Daughton et al. (2006). The leftwards ejection of medium size plasmoids can be observed in the movie of the evolution of the out of plane magnetic field component, B_z, provided as supplemental material. A zoom of the area $-102.4 < x/d_i < 102.4$, $-51.2 < y/d_i < 51.2$, is given. Magnetic field lines are shown in white. The plasmoids are the areas of strong positive B_z enclosed by magnetic field lines. Medium size plasmoids are emitted leftwards starting from $\Omega_{ci}t \sim 90$. At $\Omega_{ci}t \sim 160$, a slow ($v_x \sim -0.04 \div 0.05\ d_i\ \Omega_{ci}$) plasmoid forms at the original X point and prevents the ejection of the leftwards medium size plasmoids. The plasmoids already ejected continue moving leftwards. At time $\Omega_{ci}t = 220$, a small ($\sim 6d_i$) SS/RD compound structure is observed in the leftwards exhaust. It rapidly grows ($\sim 23.7d_i$ at $\Omega_{ci}t = 240$) and is fully developed by $\Omega_{ci}t = 250$. In the rightwards exhaust, where only small plasmoids were ejected, a similar SS/RD structure had already grown steadily from 12.5 d_i at time $\Omega_{ci}t = 180$ to 30.6 d_i at time $\Omega_{ci}t = 250$. The structure expands more rapidly than the exhaust itself: at $\Omega_{ci}t = 180$, when the rightwards exhaust is $\ell/d_i \sim 114$ long, it covers 11 % of it. At time $\Omega_{ci}t = 240$, with $\ell/d_i \sim 170$, the SS/RD is as long as

~ 18 % of the exhaust.

The SS/RD structures in the leftwards exhaust at time $\Omega_{ci}t = 250$ are analyzed here using the Rankine-Hugoniot (RH) jump relations (Goedbloed & Poedts 2004).

Figure 1 (a) shows the out of plane electron current, J_{ze}, in adimensional units, at time $\Omega_{ci}t = 250$, in a portion of the domain centered around the lower reconnection point. The normalization constants e, m_i and ω_{pi} are the electron charge, the ion mass and the ion plasma frequency. The transitions investigated are located in the leftwards exhaust and are marked by red lines. Figure 1 (b) depicts a further zoom of the area. Magnetic field lines are black, smoothed ion and electron stream lines purple and white. At the outer transitions, the ions (purple lines) sucked into the reconnection region bend in the outflow direction, while the electrons (white) are affected more severely by the presence of the separatrices (Lapenta et al. 2014). The magnetic field lines bending across the inner transitions remind of the textbook illustration of rotational discontinuities.

The Rankine-Hugoniot conditions for the four transitions are verified in the deHoffman-Teller frame. The deHoffman-Teller velocity $\mathbf{v}_{dHT}$ is calculated separately for each transition following standard analysis methods for multi-spacecraft data (Khrabrov & Sonnerup 1998). Virtual spacecraft data are obtained by randomly generating 100 couples of points at a distance $0.5 < d/d_i < 2$ up- and downstream of each of the discontinuities. $\mathbf{v}$ is the *fluid* velocity, related to the electron and ion velocities $\mathbf{v}_e$ and $\mathbf{v}_i$ as in $\mathbf{v} = \mathbf{v}_i + 1/m_r\mathbf{v}_e$. $\mathbf{U} = \mathbf{v} - \mathbf{v}_{dHT}$ is the fluid velocity in the deHoffman-Teller frame. The subscript N and $T1$ refer to the normal and in plane tangential component of a vector to the discontinuity. The components are calculated using the normal vector $\mathbf{N}$, the in plane tangential vector $\mathbf{T1}$ and, when needed, deHoffman-Teller velocity calculated for that specific transition. The normal vectors point upstream, the in plane tangential vectors in the direction which gives $\mathbf{T2} = \mathbf{T1} \times \mathbf{N}$ along the z axis. For both the slow shock and rotational discontinuity identification, two of the Rankine-Hugoniot (RH) conditions, $[B_N] = 0$ and $[\mathbf{E}_T] = 0$,

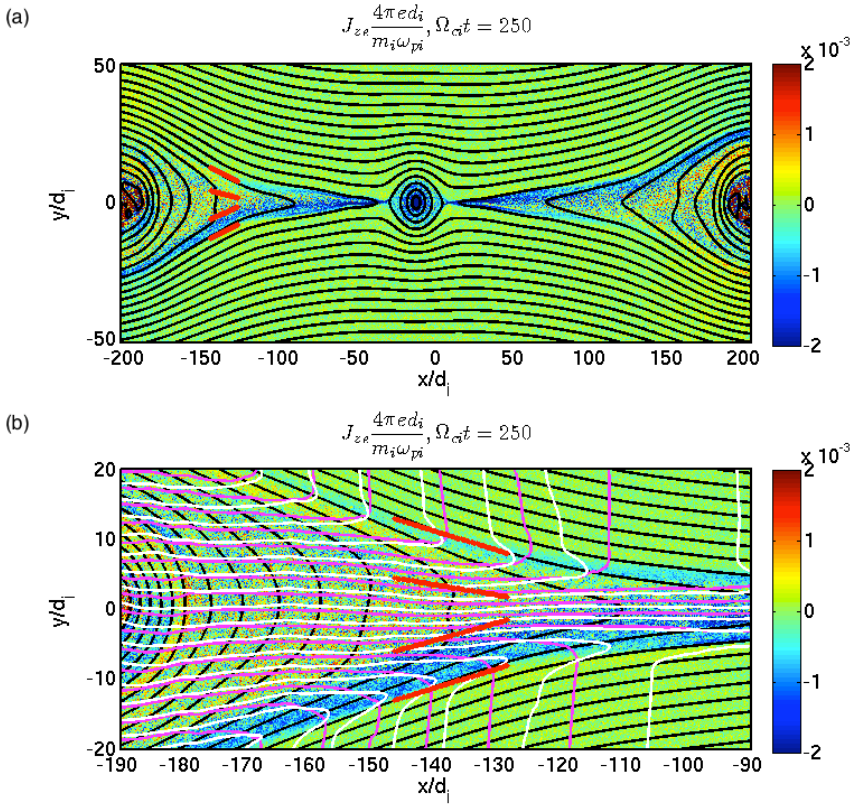

Fig. 1.— Out of plane electron current J_{ze}, in adimensional units, at time $\Omega_{ci}t = 250$ and at different zoom levels. In panel (a) and (b) the magnetic field lines are shown in black. In panel (b) only, the smoothed flow lines for electrons (white) and for ions (purple) are superimposed. The four transitions investigated are marked in red.

are preliminarily tested. Then, specific conditions for the identification of each kind of discontinuity are checked.

In Figure 2 the external transitions, identified as slow shocks, are examined. Figure 2 depicts vertical cuts of the normal component of the magnetic field (B_N, panel a), of the in plane tangential component of the electric field (E_{T1}, b) and of $-\mathbf{v} \times \mathbf{B}$ (c) at the coordinates $x/d_i = -143.1$ (red line) and $x/d_i = -132.2$ (blue line) and as a function of y. All quantities are in adimensional units. The dashed lines are the moduli of $\mathbf{B}$, $\mathbf{E}$ and $\mathbf{v} \times \mathbf{B}$ respectively and the vertical lines indicate the y position of the external discontinuities at the different x coordinates. The discontinuities have a finite width $\Delta/2 = d_{i,loc}$ (Treumann 2009) up- and down-stream of the vertical lines drawn, where $d_{i,loc}$ is the local ion skin depth. $\Delta_{SS}/2 = d_{i,loc} = 3.25$ for the slow shocks and $\Delta_{RD}/2 = d_{i,loc} = 1.6$ for the rotational discontinuities. The widths are represented as shaded areas in Figure 2 and Figure 3. The cuts, the vertical lines and the shaded areas are matched by colors. The RH conditions are considered verified if the variable is satisfactorily constant at the edges of the shaded areas. This is certainly the case for B_N, for the in plane tangential component of $(-\mathbf{v} \times \mathbf{B})_{T1}$ and for E_{T2} (not shown here), as it can be verified by comparing the quantities in panel (a) and (c) with their moduli.

In the case of E_{T1}, one can see large peaks at $\sim 1 d_i$ downstream of the lower transitions. Comparing it with $(-\mathbf{v} \times \mathbf{B})_{T1}$, it is clear that they are due to the non ideal part of the generalized Ohm's law, possibly to electron holes (Drake et al. 2003) from streaming instabilities in the separatrices (Lapenta et al. 2011; Divin et al. 2012). This reminds that the fundamental kinetic nature of the medium cannot be neglected.

Figure 2 provides evidence for the identification of the external transitions in Figure 1 as slow shocks. The variation of the in plane tangential component of the magnetic field, B_{T1}, of the mass density ρ and of the total pressure P are examined in panel (d), (e) and (f). The total pressure P is $P = 1/3\,(\,Tr\,(\mathbf{\Pi}_i) + \,Tr\,(\mathbf{\Pi}_e))$. Tr is the trace of a matrix and $\mathbf{\Pi}_i$,

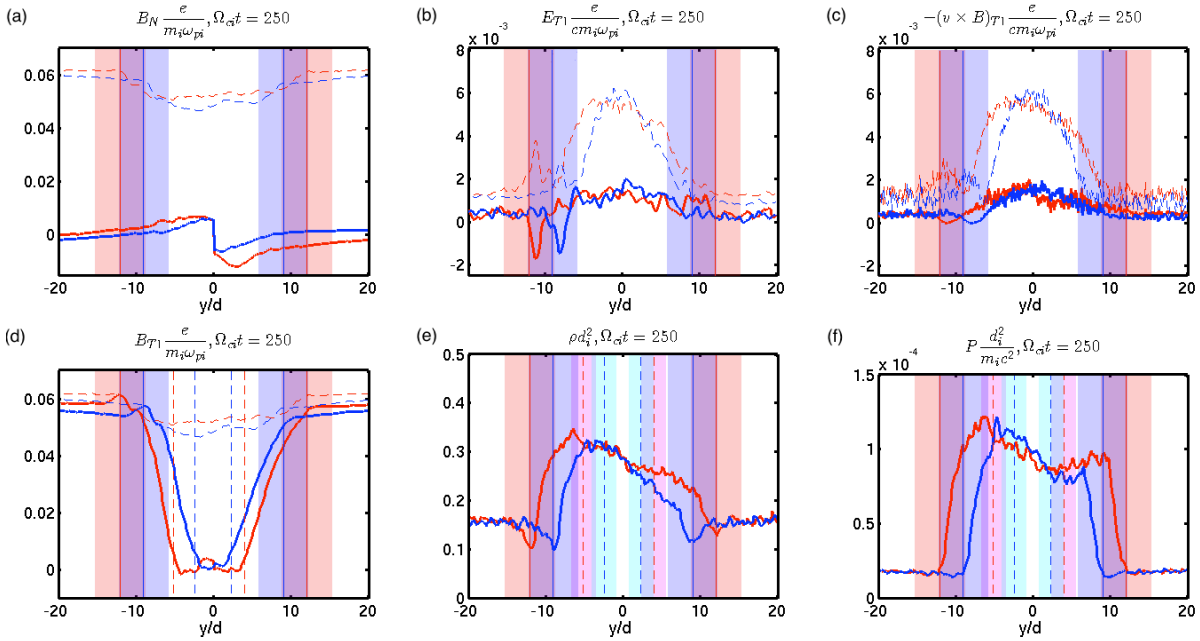

Fig. 2.— B_N (a), E_{T1} (b), $-(\mathbf{v} \times \mathbf{B})_{T1}$ (c), B_{T1} (d), mass density ρ (e) and total pressure P (f), all in adimensional units, as a function of y/d_i and at the coordinate $x/d_i = -143.1$ (red line) and $x/d_i = -132.2$ (blue line). The time is $\Omega_{ci} t = 250$. The solid vertical lines mark the y positions of the external transitions, the dashed vertical lines (when present) the positions of the internal transitions. The shaded areas mark the width of the transition they enclose. The vertical cuts, the positions of the fronts and their widths are paired by colors. The respective moduli are plotted (when present) as dashed lines.

$\mathbf{\Pi}_e$ are the pressure tensors for ions and electrons. P is used out of simplicity; the pressures for ions and electrons are significantly different, especially in correspondence of the upper separatrix, and anisotropic, with $P_{\parallel} > P_{\perp}$. Figure 2 (d) shows a strong reduction of B_{T1} downstream of the external transitions, as expected for slow shocks. Figure 2 (e) and (f) show density compression and a sharp increase of the total pressure in correspondence of the fronts.

The RH conditions $[B_N] = 0$ and $[E_{T1}] = 0$ are verified for the internal discontinuities in Figure 3 (a) and (b). Again $[E_{T2}] = 0$ is well verified but not shown.

A rotational discontinuity does not compress or heat the plasma. The magnetic field rotates, but its modulus is left unchanged. As shown in Figure 2 (e) and (f), the variation of both the density and total pressure at the edges of the internal discontinuities (vertical dashed lines, the thicknesses are marked by magenta and cyan shaded areas) is minimal if compared with the remarkable compression and heating in correspondence of the external shocks. As shown in Figure 3 (a), the magnetic field modulus (dashed line) is unaltered across the internal discontinuities. Downstream of the transitions, the in plane tangential component of the magnetic field is switched-off, giving rise to a "switch-off rotational discontinuity". The switch-off can be verified, for both B_{T1} (not depicted) and B_x (in Figure 3, panel c). $B_{T1} \sim B_x$. Horizontal lines mark the 0 and $\pm B_0/10$.

In the Walén test for rotational discontinuities, it is checked if the tangential components (along **T1** and **T2**) of the magnetic field and of the fluid velocity in the deHoffman-Teller frame rotate together by comparing the variation across the front of "observed" ($\Delta\mathbf{U}_{t,obs}$) and "theoretical" ($\Delta\mathbf{U}_{t,th}$) velocities calculated as (Retinò et al. 2005):

$$\Delta\mathbf{U}_{T,obs} = \mathbf{U}_{T,D} - \mathbf{U}_{T,U}; \Delta\mathbf{U}_{T,th} = \pm\left[(1-\alpha_U)4\pi\rho\right]^{-1/2} \cdot \left[\mathbf{B}_{T,D}(1-\alpha_D) - \mathbf{B}_{T,U}(1-\alpha_U)\right] \quad (1)$$

The subscripts U and D stand for upstream and downstream and the factor $\alpha \equiv \dfrac{\left(P_{\parallel} - P_{\perp}\right)}{(B^2/4\pi)}$ accounts for the anisotropy of the medium (Paschmann et al. 1998). Following Scudder

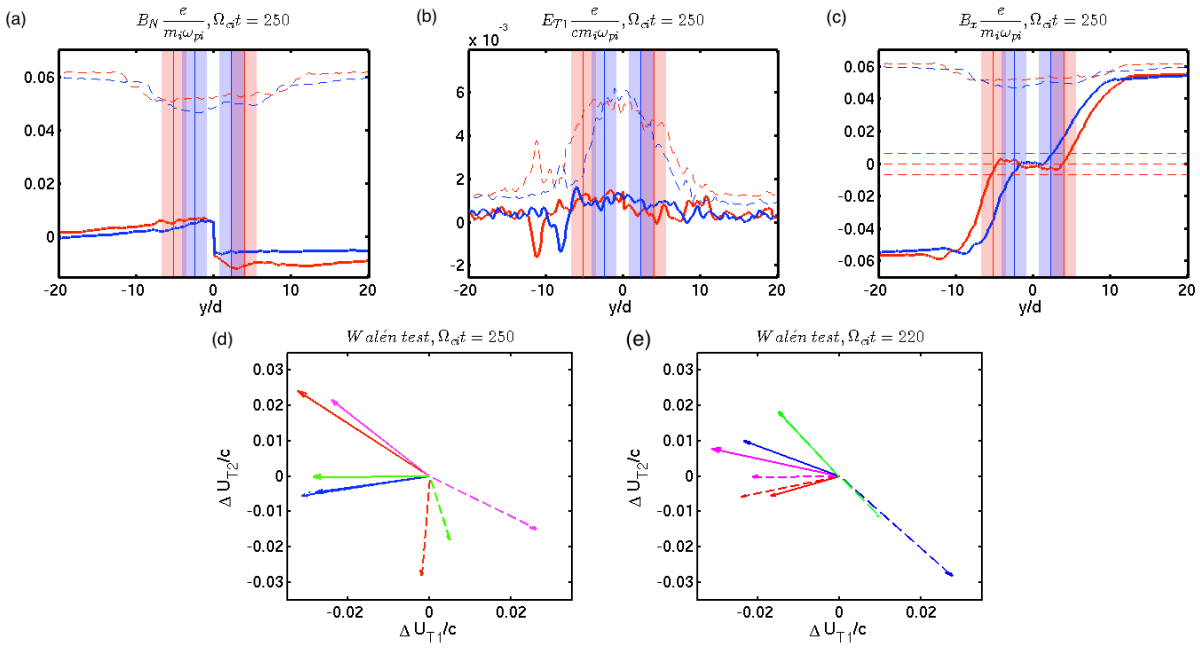

Fig. 3.— B_N (a), E_{T1} (b) and B_x (c), all in adimensional units, as a function of y/d_i and at the coordinate $x/d_i = -143.1$ (red line) and $x/d_i = -132.2$ (blue). The time is $\Omega_{ci}t = 250$. The solid vertical lines mark the y positions of the internal transitions, the shaded areas mark the width of each internal transition. In the case of B_x, the dashed lines are $-B_0/10$, 0 and $B_0/10$. Panel (d) shows the generalized Walén test for the four discontinuities (red, magenta, blue and green) in the T1-T2 plane. Panel (e) shows the generalised Walén test for the discontinuities at coordinates $x/d_i = 109.4$ and $x/d_i = 113.0$ at time $\Omega_{ci}t = 220$.

.

et al. (1999); Le et al. (2014), the generalized Walén relation is verified here. It applies to cases where the ions are not magnetized (as here upstream) and the plasma carries large currents. It substitutes the center of mass velocities with the ones of the magnetized species, the electrons. The electron pressure anisotropy is used rather than the total one. A perfectly satisfied Walén test yields $R = |\Delta \mathbf{U}_{T,obs}|/|\Delta \mathbf{U}_{T,th}| = 1$. The angle θ between the two vectors is either 0° or 180°. Figure 3 (d) shows the results of the Walén test in red, magenta, blue and green for the four discontinuities of panel a and b, from left to right. Solid (shaded) lines are the theoretical (observed) velocity variation values in the in plane (T1) and out of plane (T2) tangential directions. The calculated R's and θ's are $R = 0.67, 0.93, 1.12, 0.65$ and $\theta = 123, 168, 0.7, 105$ respectively. The generalized Walén test is excellently passed by the discontinuities at $x/d_i = -132.2$ (magenta and blue), but the results for the discontinuities at $x/d_i = -143.1$ are inconclusive. To verify the SS/RD identification hypothesis, the same analysis of Figure 2 and Figure 3, panel (a) to (d), is repeated for comparable external and internal transitions at a different location and time. The rightwards exhaust is examined at time $\Omega_{ci}t = 220$. The results for the vertical cut plots (now shown here) are comparable. The generalised Walén test is depicted in Figure 3, panel (e), for the internal transitions at the coordinates $x/d_i = 109.4$ and $x/d_i = 113.0$. The R's and θ's are 1.4, 0.66, 0.64, 1.54 and 4.42, 14.47, 178.92, 157.6 for the red ($x/d_i = 109.4$, lower RD), magenta ($x/d_i = 113.0$, lower RD), green ($x/d_i = 109.4$, upper RD) and blue ($x/d_i = 113.0$, upper RD) case. The identification of the transitions as Rotational Discontinuities-like is supported, in particular, by the values of the angles between the "theoretical" and the "observed" data.

The fact that the same structures develop at $\Omega_{ci}t = 220$ and $\Omega_{ci}t = 250$ is quite significant. At $\Omega_{ci}t = 250$, the current layer upstream the reconnection exhaust has already developed into a plasmoid chain. The identification of the SS/RD structure at a time, $\Omega_{ci}t = 220$, when the interaction of the exhaust with the plasmoid chain is negligible shows that the

SS/RD develops independently of it.

4. Discussion

This paper studies the evolution of fully kinetic simulations of collisionless magnetic reconnection at long simulated time and large domains. The aim is to understand whether this kind of simulations transition towards single X point Petschek-like states (as observed by Gosling (2007)) or towards a plasmoid-dominated current sheet (as observed by Eriksson et al. (2014)). The simulation points towards the development of a mixed scenario. Plasmoids are emitted asymmetrically into the two exhausts. The comparison between the leftwards and the rightwards exhaust shows that medium size plasmoids disrupt the formation of a Petschek-like SS/RD structure. The SS/RD structure forms earlier in the rightwards exhaust, where only small plasmoids are emitted. The SS/RD develops in the leftwards exhaust when a monster plasmoid prevents the emission of the medium size plasmoids traveling leftwards at earlier times. A switch-off condition reminding of Petshek's reconnection model then develops in both the leftwards and rightwards exhausts. It is expected to persist for times long enough (decades of Ω_{ci}) to be observable. Two slow shocks form in correspondence of the reconnection separatrices and reduce the in plane tangential component of the magnetic field. Two internal transitions reminding of rotational discontinuities ("switch-off rotational discontinuities") then perform the actual switch-off. Future work will focus on validating the observation of the SS/RD compound structure in simulations performed with more realistic parameters, i.e. an higher mass ratio and electron and ion velocities and temperatures closer to actual magnetospheric or solar wind conditions.

This work has used resources from the European Union FP7 program under Grant Agreement No 284461 - Project eHeroes, from the NASA MMS-IDS mission and from the NERSC Center, a DOE Office of Science User Facility supported by the Office of Science of the U.S. Department of Energy under Contract No. DE-AC02-05CH11231. We acknowledge PRACE for awarding us access to CURIE (grant No 2011050747) and SuperMUC (grant No 2013091928) and NASA for access to NASA NAS facilities. M.E.I. is funded by a FWO fellowship, grant No 12O5215N.

REFERENCES

Arzner, K., & Scholer, M. 2001, Journal of Geophysical Research: Space Physics (1978–2012), 106, 3827

Beck, A., Innocenti, M., Lapenta, G., & Markidis, S. 2014, Journal of Computational Physics, 271, 430 , frontiers in Computational Physics Modeling the Earth System

Birn, J., Drake, J. F., Shay, M. A., et al. 2001, Journal of Geophysical Research: Space Physics, 106, 3715

Daughton, W., Scudder, J., & Karimabadi, H. 2006, Physics of Plasmas, 13, 072101

Divin, A., Lapenta, G., Markidis, S., Newman, D., & Goldman, M. 2012, Physics of Plasmas (1994-present), 19, 042110

Drake, J., Swisdak, M., Cattell, C., et al. 2003, Science, 299, 873

Drake, J., Swisdak, M., Che, H., & Shay, M. 2006a, Nature, 443, 553

Drake, J., Swisdak, M., Schoeffler, K., Rogers, B., & Kobayashi, S. 2006b, Geophysical research letters, 33

Eriksson, S., Newman, D., Lapenta, G., & Angelopoulos, V. 2014, Plasma Physics and Controlled Fusion, 56, 064008

Goedbloed, J., & Poedts, S. 2004, Principles of magnetohydrodynamics: With applications to laboratory and astrophysical plasmas (Cambridge University Press)

Gosling, J. 2007, The Astrophysical Journal Letters, 671, L73

Gosling, J. T., Skoug, R. M., McComas, D. J., & Smith, C. W. 2005, Journal of Geophysical Research: Space Physics, 110, n/a

Harris, E. 1962, Il Nuovo Cimento (1955-1965), 23, 115

Higashimori, K., & Hoshino, M. 2012, Journal of Geophysical Research: Space Physics (1978–2012), 117

Hones, E., Baker, D., Bame, S., et al. 1984, Geophysical research letters, 11, 5

Innocenti, M., Beck, A., Ponweiser, T., Markidis, S., & Lapenta, G. 2015, Computer Physics Communications, 189, 47

Innocenti, M., Lapenta, G., Markidis, S., Beck, A., & Vapirev, A. 2013, Journal of Computational Physics, 238, 115

Ji, H., & Daughton, W. 2011, Physics of Plasmas (1994-present), 18, 111207

Karimabadi, H., Daughton, W., & Quest, K. B. 2005, Journal of Geophysical Research: Space Physics (1978–2012), 110

Karimabadi, H., Krauss-Varban, D., Omidi, N., & Vu, H. X. 1999, Journal of Geophysical Research: Space Physics, 104, 12313

Keppens, R., Porth, O., Galsgaard, K., et al. 2013, Physics of Plasmas (1994-present), 20, 092109

Khrabrov, A. V., & Sonnerup, B. 1998, Analysis Methods for Multi-Spacecraft Data, 221

Kleva, R. G., Drake, J., & Waelbroeck, F. 1995, Physics of Plasmas (1994-present), 2, 23

Krauss-Varban, D., & Omidi, N. 1995, Geophysical research letters, 22, 3271

Lapenta, G. 2008, Physical review letters, 100, 235001

Lapenta, G., Innocenti, M., Markidis, S., et al. 2014 - accepted, Advances in Engineering Software

Lapenta, G., Markidis, S., Divin, A., Goldman, M., & Newman, D. 2011, Geophysical Research Letters, 38

Lapenta, G., Markidis, S., Divin, A., Newman, D., & Goldman, M. 2014, arXiv preprint arXiv:1406.6141

Le, A., Egedal, J., Ng, J., et al. 2014, Physics of Plasmas (1994-present), 21, 012103

Le, A., Egedal, J., Ohia, O., et al. 2013, Phys. Rev. Lett., 110, 135004

Lin, J., Cranmer, S., & Farrugia, C. 2008, Journal of Geophysical Research: Space Physics (1978–2012), 113

Lin, Y., & Swift, D. W. 1996a, Journal of Geophysical Research: Space Physics (1978–2012), 101, 19859

—. 1996b, Journal of Geophysical Research: Space Physics, 101, 19859

Liu, Y.-H., Drake, J. F., & Swisdak, M. 2012, Physics of Plasmas (1994-present), 19,

Lottermoser, R.-F., Scholer, M., & Matthews, A. 1998, Journal of Geophysical Research: Space Physics (1978–2012), 103, 4547

Loureiro, N., Samtaney, R., Schekochihin, A., & Uzdensky, D. 2012, Physics of Plasmas (1994-present), 19, 042303

Loureiro, N., Schekochihin, A., & Cowley, S. 2007, arXiv preprint astro-ph/0703631

Markidis, S., Henri, P., Lapenta, G., et al. 2013, Physics of Plasmas (1994-present), 20, 082105

Markidis, S., Lapenta, G., et al. 2010, Mathematics and Computers in Simulation, 80, 1509

Nakamura, M., Fujimoto, M., & Maezawa, K. 1998, Journal of Geophysical Research: Space Physics (1978–2012), 103, 4531

Olshevsky, V., Lapenta, G., & Markidis, S. 2013, Physical review letters, 111, 045002

Paschmann, G., Fazakerley, A. N., & Schwartz, S. J. 1998, Analysis methods for multi-spacecraft data, 125

Priest, E., & Forbes, T. 2007, Magnetic Reconnection, by Eric Priest, Terry Forbes, Cambridge, UK: Cambridge University Press, 2007, 1

Retinò, A., Cattaneo, M. B., Marcucci, M., et al. 2005in , 461–473

Ricci, P., Brackbill, J., Daughton, W., & Lapenta, G. 2004, Physics of plasmas, 11, 4102

Sato, T., & Hayashi, T. 1979, Physics of Fluids (1958-1988), 22, 1189

Scudder, J., Puhl-Quinn, P., Mozer, F., Ogilvie, K., & Russell, C. 1999, Journal of Geophysical Research: Space Physics (1978–2012), 104, 19817

Treumann, R. 2009, The Astronomy and Astrophysics Review, 17, 409

Uzdensky, D., Loureiro, N., & Schekochihin, A. 2010, Physical review letters, 105, 235002

Vasyliunas, V. M. 1975, Reviews of Geophysics, 13, 303